RSC Advances

Effective Improvement of the Photovoltaic Performance of Black Dye Sensitized Quasi-Solid-State Solar Cells

SCHOLARONE™
Manuscripts

Journal Name

RSC Advances

ARTICLE TYPE

Effective Improvement of the Photovoltaic Performance of Black Dye Sensitized Quasi-Solid-State Solar Cells

Shuai Chang,[a] King Young Wong,[a] Xudong Xiao[a] and Tao Chen*[a]

To solve the energy crisis in the future, one of the most promising ways is to convert sunlight into electricity by solar cell. A high quality solar device should simultaneously meet the 10 requirements of high efficiency, low cost, long-term stability as well as the environmental friendliness in terms of both materials sources and processing. Unfortunately, there has been no such kind of solar cell that can satisfy all the requirements. Therefore, researchers have made continued efforts into the development of 15 new device structures as well as fabrication techniques. The third-generation excitonic solar cells, such as dye (quantum dot)-sensitized solar cells, organic (polymer) solar cells and perovskite based solar cells,[1-7] possess low fabrication cost while they suffer from either poor long-term stability or low solar-to-electrical 20 power conversion efficiency (PCE). However, due to the potential low cost for future industrial productions, increasing attention has been paid to the overall performance improvement.

Dye-sensitized solar cells (DSSCs) take advantage of dye molecules for light absorption; they can be fabricated with liquid 25 or quasi-solid-state electrolyte or solid-state hole transporting materials (HTM).[8-17] In terms of device fabrication, liquid electrolyte infill is usually conducted by a convenient injection approach. Nevertheless, the electrolyte leakage and dye dissociation into liquid electrolyte are significant degradation 30 mechanisms in this type of device structure.[18] The corrosion on the counter electrode is also a main concern in the application of liquid electrolyte. The use of solid-state hole transporting materials (HTM) can significantly improve the device stability and avoid the problems,[19] while the infiltration of HTM is usually 35 conducted by spin coating, which poses severe challenge in the large area production. Furthermore, the spin coating process also causes considerable materials loss. Quasi-solid-state gel electrolyte based device show long-term stability and infiltration of the electrolyte can be conducted by the conventional injection 40 method,[20-23] which possesses the advantages of both liquid and solid-state devices. In specific, once the electrolyte heated up to around 100 ^{o}C, it is transformed to fluidic state which allows facile injection. When fluidic electrolyte cooling down to room temperature, it transforms back to pseudo-solid-state. Compared 45 with the liquid electrolyte and solid state HTM based DSSCs, however, quasi-solid-state DSSCs are less investigated.

In DSSC, dye molecule plays the role as light harvester, and the light harvesting efficiency sets the threshold of final PCE. To date, several classes of molecular sensitizers have been developed 50 such as ruthenium complexes based dyes (e.g. **N719**, **N3** and **N749**), porphyrin based molecules as well as the organolead perovskite based materials.[1, 2, 8, 24] Notably, only the **N749** dye (black dye) can extend the light absorption to the red and near-infrared (NIR) range, which provides possibility for high

55 efficiency light harvesting. **N749** has been widely used in the liquid electrolyte based DSSCs,[25-27] while it is rarely seen in the quasi-solid-state devices. To take full advantage of the **N749** dye molecules, for the first time we apply it for the sensitization of quasi-solid-state solar cells and explore the coadsorption of small 60 organic sensitizers for the performance improvement.
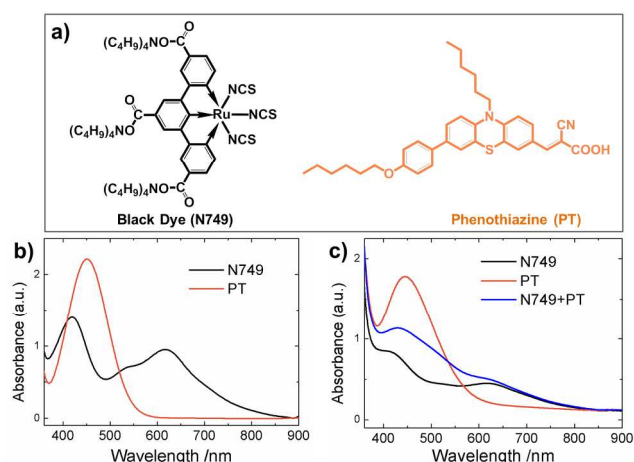
Fig. 1 (a) Molecular structures of black dye (**N749**) and phenothiazine based dye (**PT**) (b) UV-Vis absorption of **N749** and **PT** in THF solution and (c) **N749**, **PT** and **N749+PT** co-adsorbed on TiO$_2$ films (thickness 3 μm)

The UV-Vis-NIR absorption of the **N749** solution shows typical absorption spectra ranging from visible to NIR (~900 nm) (Fig. 1a, 1b), the dye-anchored TiO$_2$ nanoparticle mesoporous film also presents light absorption to NIR region (Fig. 1c). With 65 this broad spectral response, it is of great interesting in the liquid electrolyte based DSSCs and showed high photovoltaic performance, the PCE can reach around 11%.[25-27] In the fabrication of quasi-solid-state DSSCs, we assemble the dye-soaked film into DSSC by stacking with Pt sputtered counter 70 electrode separated by a thermal melting film. The quasi-solid electrolyte is injected through the holes predrilled in the counter electrode using an injection-and-evacuation fashion according to our reported method.[23] It was finally sealed with a melting parafilm. The effective areas of the devices are controlled to be 75 0.196 cm^2. The optimization shows that the anode film composed of 12 μm of transparent layer and 6 μm of scattering layer generate highest PCE of 6.32% (device **1**), with short-circuit current density (J_{sc}) of 13.76 mA cm^{-2}, open-circuit voltage (V_{oc}) of 0.632 V and fill factor (FF) of 72.7%.

In our previous investigation we found that the postadsorption of small molecules into the interstitial site of porphyrin sensitized anode films can significantly reduce the back reaction from the electrons on the conduction band of TiO_2 and I_3^- species in the electrolyte.[28] If the small molecules are dye sensitizers, the spectral response of the device can also be improved. Herein, we apply this method to improve the light harvesting of ruthenium based dye molecules. A phenothiazine-based dye (Fig. 1a, **PT**) is applied, which is synthesized according to our reported method.[29] The absorption spectrum shows that **PT** presents one broadened absorption peak from blue end to ~560 nm. It also noted that the absorption of **N749** in the blue region (~450 nm) is relatively weak (Fig. 1b and 1c). When they are coadsorbed on the anode film, the light absorption is able to be significantly improved (Fig. 1c). Therefore, the combination of these two kinds of dye molecules can be expected to improve the spectral response of the DSSCs.

A stepwise dye-loading method was used for the co-sensitization. For comparison, DSSC individually sensitized by **PT** (device **2**) were also prepared, showing PCE of 6.5% (Fig. 2a). In the cosensitized devices, optimization shows that the dye soaking in **N749** for 8 h, followed by immersing it in **PT** for 3 h can generate highest PCE of 8.0% (device **3**), with J_{sc} of 17.59 mA cm^{-2} and V_{oc} of 0.645 V (Fig. 2a). The photovoltaic parameters of all devices are summarized in Table 1 for easy reference. It can be concluded that after the adsorption of **PT**, the **N749**-sensitized device show remarkable efficiency enhancement.

To investigate the wavelength dependent light response of the devices, we performed incident photon-to-electron conversion efficiency (IPCE) characterization (Fig. 2b). The IPCE is associated with the product of light harvesting efficiency (η_{lh}), charge injection efficiency (η_{inj}), and charge collection efficiency (η_{coll}). From Fig. 2b, the IPCE spectrum of **N749**-sensitized device stretches from the visible light range to nearly 900 nm, which shows the typical photocurrent generation behaviour of the **N749**. The IPCE of cosensitized device is boosted in a broad wavelength similar to the black dye while exhibits a huge hump in 400–600 nm, this improvement is attributed to the **PT** dye molecules. Therefore, the significantly improved J_{sc} in the cosensitized device (17.59 mA cm^{-2}) is mainly due to the improved light harvesting, which is consistent with the UV-visible spectra alternations where the co-sensitized film presents increased light absorption, especially at the absorption peaks of **PT** (Fig. 1b). The V_{oc} of the co-sensitized device **3** (0.645 V) falls in between those of the devices sensitized by solely **N749** (0.632 V) and **PT** (0.721 V).

In the process of optimization, we also tried the cocktail dye-loading approach that is to blend the two dyes together in acetonitrile/tert-butyl alcohol (1:1, v/v) solution for dye adsorbing, denoted as device **4**. The IPCE of device **4** in Fig. 2b shows that the performance of **N749** is quite low compared to the optimized device **3**, the characteristic region of **N749** from 600 nm-900 nm becomes much lower, while the characteristic region of **PT** around 470 nm is a little higher. The final PCE is only 6.6%, showing negligible improvement when compared with the devices individually sensitized by **N749** and **PT**.

Therefore, the stepwise method is an appropriate strategy for dye co-sensitization in this case. Detailed inspection shows that the IPCE of co-sensitized device **3** from 610 nm to 900 nm remains nearly unchanged compared with that of individually sensitized device **1**, revealing that the post-adsorption of small organic dye would not cause detachment of pre-adsorbed **N749** molecules. Therefore, by first incubating the **N749** dye for an enough timespan to reach its saturated dye-loading concentration,
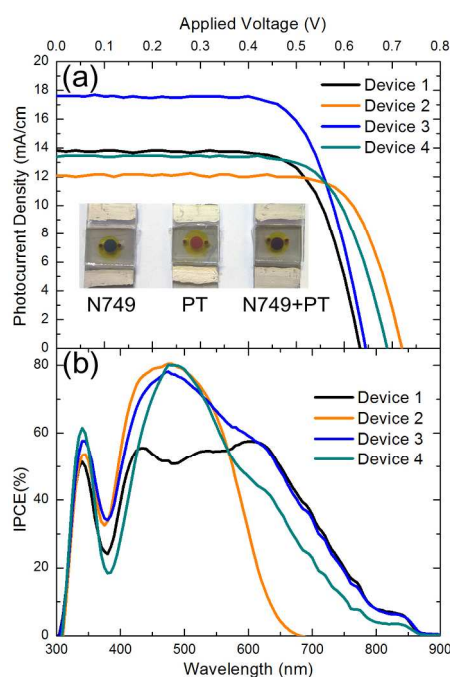
Fig. 2 (a) Photocurrent-voltage (*J-V*) characteristics and (b) the corresponding incident photon-to-electron conversion efficiency spectra of devices sensitized by **N749**, **PT** and **N749+PT** (co-sensitized using stepwise and cocktail methods, respectively) under the same fabrication and characterization conditions. The inset in Fig. 2(a) shows the optical images of **N749**, **PT** and **N749+PT** cosensitized devices.

we successfully avoid the competition in the cocktail dye-loading circumstance, obtaining an optimized the dye-loading process.

Table 1 J_{sc}, V_{oc}, fill factor (*FF*) and PCE (η) parameters of device **1** to **4** measured under one sun illumination (AM 1.5 G)

Device[1]	Dye	Dye-loading strategy	J_{sc} (mA/cm^2)	V_{oc} (V)	FF (%)	η (%)
1	N749	N/A	13.76	0.632	72.7	6.3
2	PT	N/A	12.08	0.721	75.1	6.5
3	N749+PT	Stepwise	17.59	0.645	70.0	8.0
4	N749+PT	Cocktail	13.49	0.69	71.2	6.6
5	PT+porphyrin[2]	Stepwise	18.61	0.70	70.5	9.2

[1] the effective areas of all the devices are 0.196 cm^2; [2] the molecular structure of porphyrin is provided in the Supporting Information.

To further justify the advantage of sequential dye soaking method for the efficiency improvement in the quasi-solid-state DSSCs, we fabricated another set of devices using the **PT** co-absorbed with a zinc porphyrin based dye (ZnP).[28] Details are provided in the Supporting Information. *J-V* characteristics and IPCE spectra are also performed and presented in Fig. S1 and Table S1. Remarkable results show that the PCE of the co-sensitized device is boosted to 9.2% (device **5**, Table 1), which is comparable to the highest PCE in literature in quasi-solid-state DSSCs (9.1%).[30] In addition, the device solely sensitized by porphyrin molecule gives a PCE of 6.5% (Fig. S1 and Table S1).

To gain insight into the charge transfer behaviour of the devices (co)sensitized by **N749** and **PT**, we performed electrochemical impedance spectra (EIS) under the dark
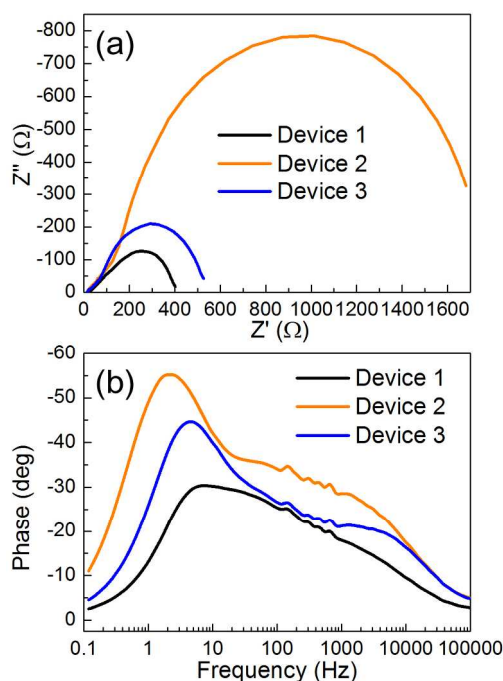
Fig. 3 (a) Nyquist and (b) Bode phase plots of DSSCs based on individual **N749** and **PT** electrode (device **1** and **2**) and **N749** + **PT** co-sensitized electrodes (device **3**)

conditions. As shown in Fig. 3a, the interception of EIS curves on the *x*-axis indicates the resistance of FTO glass surface. The straight lines at high frequencies imply ion diffusion resistance through the 3D anode network. They are overlapped, indicating
5 similar ion transport speed in the devices. Further, the Nyquist arcs appeared at intermediate-frequency regime are associated with the recombination resistance (R_{ct}) at the interface of TiO$_2$/dye/electrolyte, i.e., the recombination kinetics between conduction-band electrons in TiO$_2$ and I$_3^-$ species from the
10 electrolyte. The calculated resistance values (R_{ct}) are listed in Table S2; the larger the R_{ct}, the slower the recombination kinetics. It is noted that device **2** presents the largest R_{ct} (1592.6 Ω, Table S2). This is because the small molecular can form densely packed monolayer on the TiO2 surface which can much
15 more effectively supress the back charge transfer.[31] This result contributes to the higher V_{oc} of **PT** sensitized device. Also, the lowest V_{oc} of **N749**-sensitized device can be explained by its smallest R_{ct} (287.2 Ω). The large molecules usually form less densely packed monolayer due to the steric repulsion, thus
20 leading to more available site on the TiO$_2$ surface for I$_3^-$ approaching. Furthermore, the calculated R_{ct} of co-sensitized device **3** is 443.1 Ω, in the middle of device **1** and **2**. This observation is consistent with the V_{oc} evolution as discussed above.
25　　On the other hand, from the Bode phase plots of the devices (Fig. 3b), the characteristic back charge transfer frequency (*f*) can be obtained, which corresponds to the peak of the Bode phase plot. The electron lifetime (τ_n) in the TiO$_2$ film can be calculated from Eq. (1):

30
$$\tau_n = \frac{1}{2\pi f} \qquad (1)$$

where *f* is the characteristic frequency, corresponding to the peak in intermediate-frequency regime. The obtained τ_n values are also shown in Table S1. It can be seen that the device sensitized by **N749** alone displays the shortest τ_n among all the devices.
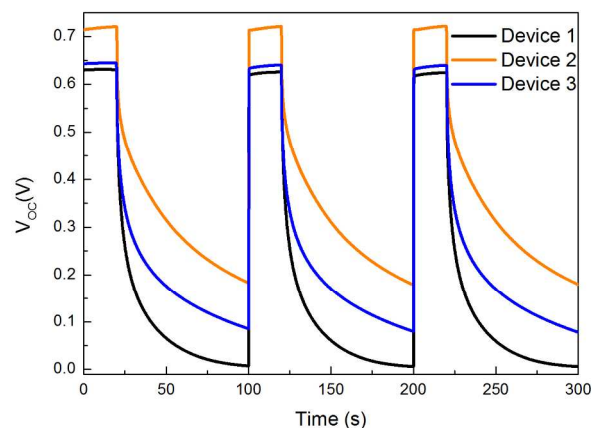
Fig. 4 Open-circuit voltage decay profiles of device **1** to **3**

35 While that with the co-adsorption of **PT**, the electron lifetime is prolonged, quite close to that of the individual **PT** sensitized device.
　　To further probe the recombination kinetics of the devices, open-circuit voltage decay (OCVD) curves were recorded, which
40 can continuously record the lifetime of V_{oc} from a steady state to dark equilibrium.[32] Fig. 4 shows the OCVD profiles of devices **1** to **3**. First the decay rate of the devices is quite slow, suggesting a reduced recombination rate in the quasi-solid state DSSCs. The correlation between V_{oc} decay and electron lifetime (τ_n') can be
45 expressed by Eq. (2):

$$\tau_n' = -\frac{K_B T}{e}\left(\frac{dV_{oc}}{dt}\right)^{-1} \qquad (2)$$

where K_B is the Boltzmann constant, *T* is temperature, and *e* is the electron charge. Therefore, the electron lifetimes can be extracted from the initial slope of V_{oc} decay curves. Firstly, the decay
50 curves of device **1** presents the steepest slope while device **2** display the slowest one, which suggest the shortest electron lifespan of **N749**-sensitized device and the longest one of **PT**sensitized device. This variation matches well with the photovoltaic and EIS analysis of the devices sensitized by the two
55 dyes.
　　In conclusion, we have demonstrated for the first time panchromatic light harvesting by using black dye in quasi-solid-state dye-sensitized solar cells. To further improve the performance, a small organic dye is inserted into the interstitial
60 site of black dye on the TiO$_2$ surface. The overall performance for the **N749** and **PT** co-sensitized device is improved by 27% and 23% with respect to individual dye-sensitized devices. The device performance improvement is mainly due to the enhanced light harvesting in the short-wavelength region and reduced back
65 charge transfer. Quasi-solid-state dye-sensitized solar cells possess unique advantages in the practical applications in terms of long-term stability, low cost and facile fabrication. The colorfulness and semitransparency are especially attractive in the building integrated photovoltaics. Our method in extending the
70 spectral response and boosting the energy conversion efficiency would facilitate the future practical applications.

Experimental

Materials:

All chemical reagents were used without further purification. Dye
75 sensitizer N749, TiO$_2$ paste were purchased from Dyesol company. PT molecule was synthesized according to our reported

method.[29] Chenodeoxycholic acid (≥97%) was purchased from Sigma Aldrich. Gel electrolyte containing I_3^-/I^- is prepared according to the reported method with minor modifications.[21]

Device fabrication:

A layer of ca. 6 μm TiO_2 paste (20 nm in diameter) was printed onto the FTO conducting glass and then dried for 6 min at 150 °C. This procedure was repeated two times to prepare a thickness of ca. 12 μm and the resulting surface was finally coated by a scattering layer (ca. 6 μm) of TiO_2 paste (200 nm). The final thickness of the electrodes is ca. 18 μm. These TiO_2 electrodes were gradually heated under an air flow at 275 °C for 5 min, 325 °C for 5 min, 375 °C for 5 min, 470 °C for 30 min to remove polymers. Afterwards, these sintered films were soaked with 0.02 M TiF_4 aqueous solution for 60 min at 70°C, washed with deionized water, further annealed at 450 °C for 30 min. The black dye (N749, 0.2 mM) and deoxycholic acid (DCA, 10 mM) were dissolved in acetonitrile/tert-butyl alcohol (1:1, v/v) solution; and the organic dye (PT, 0.5 mM) was also dissolved in acetonitrile/tert-butyl alcohol (1:1, v/v) solution. After cooling down to ca. 80 °C, the electrodes of device 1 and 2 were immersed in N749 solution and PT solution, respectively. They were placed for 12 h to reach enough dye loading for the maximum efficiency. The electrodes of device 3 were all firstly soaked in N749 solution for 8 h, and then they were transferred into PT solution for 3 h. The electrode of device 4 was immersed in a cocktail solution of 0.2 mM N749 and 0.5 mM PT for enough timespan to reach a stable dye loading state. Subsequently, the electrodes were rinsed with ethanol to remove the non-adsorbed dyes and dried in air. Pt counter electrodes were prepared by sputtering method at 15 mA for 90 s at a power 150W. Two holes (0.75 mm in diameter) were pre-drilled in the FTO glass for introducing electrolyte. The dye-adsorbed TiO_2 electrode and Pt-counter electrode were assembled into a sandwich type cell and sealed with a hot-melt film (SX1170, thickness 60 μm) at ca. 100 °C. The quasi-solid electrolyte was introduced into the cell through the drilled holes in the back of the counter electrode using an injection and purge method and relaxed at 60 °C for 30 min before cooling down to room temperature. At last, the holes were sealed by parafilm and covering glass (0.1 mm thickness) at elevated temperature. The effective areas of all the TiO_2 electrodes were 0.196 cm^2.

Characterizations:

Absorption spectra in the UV-vis region were carried out using Hitachi U-3501 UV–visible/NIR spectrophotometer. The current-voltage (*J-V*) characteristics of the assembled cells were measured by a semiconductor characterization system (Keithley 236) at room temperature in air under the spectral output from solar simulator (Newport) using an AM 1.5G filter with a light power of 100 mW/cm^2. IPCEs of DSSCs were recorded in Solar Cell QE/IPCE Measurement System (Zolix Solar Cell Scan 100) using DC mode. Electrochemical impedance spectroscopy (EIS) measurements were carried out by applying bias of 700 mV under dark condition over a frequency range of 0.1-10^5 Hz and AC amplitude of 10 mV. The parameters were calculated from Z-View software (v2.1b, Scribner AssociatNe, Inc.). For the open-circuit voltage decay (OCVD) measurements, the cell was first illuminated for 20 sec to a steady voltage, then the illumination was turned off for 80 sec and the OCVD curve was recorded, this process was repeated for three periods to further confirm the stability of the OCVD. The above two measurements were performed on a CHI 660D electrochemical workstation.

Acknowledgements

Notes and references

Department of Physics, The Chinese University of Hong Kong, Shatin, Hong Kong, China. Fax: 852- 2603 5204; Tel: 852-3943 6278; E-mail: taochen@phy.cuhk.edu.hk (T. C).

† Electronic Supplementary Information (ESI) available: additional *J-V* curves, IPCE spectra and electrochemical characterizations are provided. See DOI: 10.1039/b000000x/

1 J. Burschka, N. Pellet, S. J. Moon, R. Humphry-Baker, P. Gao, M. K. Nazeeruddin and M. Gratzel, *Nature*, 2013, **499**, 316.
2 M. Z. Liu, M. B. Johnston and H. J. Snaith, *Nature*, 2013, **501**, 395.
3 W. Zeng, G. J. Fang, T. Y. Han, B. R. Li, N. S. Liu, D. S. Zhao, Z. Q. Liu, D. Y. Wang, X. Z. Zhao and D. C. Zou, *J. Power Sources*, 2014, **245**, 456.
4 D. H. Wang, D. Y. Kim, K. W. Choi, J. H. Seo, S. H. Im, J. H. Park, O. O. Park and A. J. Heeger, *Angew. Chem. -In. Ed.*, 2011, **50**, 5519.
5 B. E. Hardin, H. J. Snaith and M. D. McGehee, *Nature Photonics*, 2012, **6**, 162.
6 S. Mathew, A. Yella, P. Gao, R. Humphry-Baker, B. F. E. Curchod, N. Ashari-Astani, I. Tavernelli, U. Rothlisberger, M. K. Nazeeruddin and M. Gratzel, *Nat. Chem.*, 2014, **6**, 242.
7 H. T. Mandalia, V. K. Jain and B. N. Pattanik, *Res. J. Chem. Sci.*, 2012, **2**, 89.
8 A. Hagfeldt, G. Boschloo, L. C. Sun, L. Kloo and H. Pettersson, *Chem. Rev.*, 2010, **110**, 6595.
9 J.-H. Yum, T. W. Holcombe, Y. Kim, K. Rakstys, T. Moehl, J. Teuscher, J. H. Delcamp, M. K. Nazeeruddin and M. Grätzel, *Sci. Rep.*, 2013, **3**.
10 J. He, L. T. L. Lee, S. Yang, Q. Li, X. Xiao and T. Chen, *Acs Appl. Mater. & Interfaces*, 2014, **6**, 2224.
11 T. Chen, W. Hu, J. Song, G. H. Guai and C. M. Li, *Adv. Funct. Mater.*, 2012, **22**, 5245.
12 S. Chang, Q. Li, X. Xiao, K. Y. Wong and T. Chen, *Energy Environ. Sci.*, 2012, 9444.
13 L. T. L. Lee, J. He, B. Wang, Y. Ma, K. Y. Wong, Q. Li, X. Xiao and T. Chen, *Sci. Rep.*, 2014, **4**.
14 P. Docampo, A. Hey, S. Guldin, R. Gunning, U. Steiner and H. J. Snaith, *Advanced Functional Materials*, 2012, **22**, 5010.
15 C. K. Xu, J. M. Wu, U. V. Desai and D. Gao, *Nano Letters*, 2012, **12**, 2420.
16 J. Yang, P. Ganesan, J. Teuscher, T. Moehl, Y. J. Kim, C. Yi, P. Comte, K. Pei, T. W. Holcombe, M. K. Nazeeruddin, J. Hua, S. M. Zakeeruddin, H. Tian and M. Grätzel, *J. Am. Chem. Soc.*, 2014.
17 G. H. Guai, Q. L. Song, C. X. Guo, Z. S. Lu, T. Chen, C. M. Ng and C. M. Li, *Solar Energy*, 2012, **86**, 2041.
18 N. Heo, Y. Jun and J. H. Park, *Sci. Rep.*, 2013, **3**.
19 U. Bach, D. Lupo, P. Comte, J. E. Moser, F. Weissortel, J. Salbeck, H. Spreitzer and M. Gratzel, *Nature*, 1998, **395**, 583.
20 Y. Bai, Y. M. Cao, J. Zhang, M. Wang, R. Z. Li, P. Wang, S. M. Zakeeruddin and M. Gratzel, *Nature Mater.*, 2008, **7**, 626.
21 P. Wang, S. M. Zakeeruddin, J. E. Moser, M. K. Nazeeruddin, T. Sekiguchi and M. Gratzel, *Nature Mater.*, 2003, **2**, 402.
22 C. Cheng, Y. Shi, C. Zhu, W. Li, L. Wang, K. K. Fung and N. Wang, *Phys. Chem. Chem. Phys.*, 2011, **13**, 10631.

23 B. Wang, S. Chang, L. T. L. Lee, S. Zheng, K. Y. Wong, Q. Li, X. Xiao and T. Chen, *Acs Appl. Mater. & Interfaces*, 2013, **5**, 8289.

24 L.-L. Li and E. W.-G. Diau, *Chem. Soc. Rev.*, 2013, **42**, 291.

25 M. K. Nazeeruddin, P. Pechy, T. Renouard, S. M. Zakeeruddin, R. Humphry-Baker, P. Comte, P. Liska, L. Cevey, E. Costa, V. Shklover, L. Spiccia, G. B. Deacon, C. A. Bignozzi and M. Gratzel, *J. Am. Chem. Soc.*, 2001, **123**, 1613.

26 Y. Chiba, A. Islam, R. Komiya, N. Koide and L. Han, *Appl. Phys. Lett.*, 2006, **88**, 223505.

27 L. Han, A. Islam, H. Chen, C. Malapaka, B. Chiranjeevi, S. Zhang, X. Yang and M. Yanagida, *Energy & Environ. Sci.*, 2012, **5**, 6057.

28 S. Chang, H. Wang, Y. Hua, Q. Li, X. Xiao, W.-K. Wong, W. Y. Wong, X. Zhu and T. Chen, *J. Mater. Chem. A*, 2013, **1**, 11553.

29 Y. Hua, S. Chang, D. Huang, X. Zhou, X. Zhu, J. Zhao, T. Chen, W.-Y. Wong and W.-K. Wong, *Chem. Mater.*, 2013, 2146.

30 Q. J. Yu, C. L. Yu, F. Y. Guo, J. Z. Wang, S. J. Jiao, S. Y. Gao, H. T. Li and L. C. Zhao, *Energy & Environ. Sci.*, 2012, **5**, 6151.

31 J. C. Love, L. A. Estroff, J. K. Kriebel, R. G. Nuzzo and G. M. Whitesides, *Chem. Rev.*, 2005, **105**, 1103.

32 A. Zaban, M. Greenshtein and J. Bisquert, *ChemPhysChem*, 2003, **4**, 859.